A self-consistent, conserving theory of the attractive Hubbard model in two dimensions

1998 J. Phys.: Condens. Matter 10 6931

(http://iopscience.iop.org/0953-8984/10/31/011)

J. Phys.: Condens. Matter **10** (1998) 6931–6951. Printed in the UK PII: S0953-8984(98)91578-8

A self-consistent, conserving theory of the attractive Hubbard model in two dimensions

M Letz† and R J Gooding

Department of Physics, Queen's University, Kingston, ON, Canada K7L 3N6

Received 11 February 1998, in final form 30 April 1998

Abstract. We have investigated the attractive Hubbard model in the low-density limit for the 2D square lattice using the ladder approximation for the vertex function in a self-consistent, conserving formulation. In the parameter region where the on-site attraction is of the order of the bandwidth, we found no evidence of a pseudo-gap. Furthermore, we have observed that the suppression of the Fermi surface known to destroy superconductivity in one and two dimensions, when these systems are treated using a non-self-consistent theory (Schmitt-Rink, Varma C M and Ruckenstein A E 1989 *Phys. Rev. Lett.* **63** 445), does not occur when pair–pair interactions are included. However, we do find a quasi-particle lifetime that varies linearly with temperature, which is similar to the findings from many experiments. Thus, although this system has a Fermi surface, it shows non-Fermi-liquid-type behaviour over a wide temperature range. We stress that our work uses thermal Green's functions along the real-time axis, and thus allows for a more accurate determination of the dynamical properties of a model than theories that require extrapolations from the imaginary-frequency axis.

1. Introduction

The high-temperature superconductors show remarkable deviations from Fermi-liquid behaviour in their normal state above T_c, the superconducting transition temperature. Although this seems to be experimentally well established, no consistent microscopic theoretical explanation has been found.

There are a number of major differences from usual metallic (BCS-type) superconductors on which we concentrate to achieve a theoretical understanding. The first one is the low dimensionality. For example, the normal-state conductivity mainly takes place in the two-dimensional (d dimensions will be denoted by dD throughout this paper) copper oxide planes. The second difference is the extremely short coherence length of the Cooper pairs in the superconducting state. These are known to be of the order of 20 Å (3–4 lattice constants), and therefore much smaller than in usual superconductors ($\sim$1000 Å). This fact, together with the extremely low ('bad metals') quasi-particle density leads to pairs which are barely overlapping ($\sim 10^{-2}$ pairs/coherence volume) with each other. Such arguments were first stated in detail by Randeria [1] who investigated conditions for a crossover between superconductivity and Bose condensation of pairs of electrons. The small overlap is claimed to be related to a separation of a temperature T^*, at which pairing takes place, from the temperature T_c, at which phase coherence and therefore superconductivity is established. In contrast to this, usual superconductors have $\sim 10^6$ pairs/coherence volume, which is believed

† Present address: Institut für Physik, Johannes-Gutenberg Universität, 55099 Mainz, Germany.

0953-8984/98/316931+21$19.50

to be why pairing and phase coherence take place at the same temperature, the mean-field T_c. Another unusual property of the cuprate superconductors is the linear resistivity in the normal state of the optimally doped materials. An ideal Fermi liquid should show a resistivity caused by electron–electron scattering near the Fermi surface which varies quadratically with the temperature. On the other hand, a crossover to a linear resistivity due to phonons is expected to take place at much higher temperatures, above the Debye temperature.

Finally, one last observation that we wish to focus on is the presence of a pseudo-gap. This feature was first observed with NMR [2–4] by measuring the spin–lattice relaxation rate for the ^{65}Cu nucleus. The relaxation rate, $1/(T_1T)$, which is temperature independent in normal metals, decreases strongly with decreasing T even above T_c for the high-T_c cuprates. The pseudo-gap has also been measured by optical experiments where it is found in the temperature dependence of the scattering time obtained from a generalized Drude theory for optical conductivity data [5, 6]. The momentum dependence of the pseudo-gap has been investigated with recent ARPES experiments, and it is found to be present mainly along the $(k, 0)$ direction, consistently with the proposed d-wave symmetry of the superconducting order parameter. It has also been observed by tunnelling (STM) [7] measurements. At present, there is ongoing discussion addressing the notion that the gap can be related to pair formation, or other possible precursor phenomena of superconductivity, which takes place at temperatures above that at which macroscopic phase coherence is established.

The above-mentioned ideas have led us to consider a simple model system in 2D which can describe short-coherence-length pairs which might exist as preformed pairs above T_c. This model, the attractive Hubbard model, for on-site, s-wave pairing only, allows us to focus on many of the above-mentioned properties. In particular, we have examined the dynamical properties of this model to see whether the attractive Hubbard model in 2D possesses a pseudo-gap. Furthermore, we have examined the temperature dependence of the imaginary part of the single-particle self-energy to learn how the scattering rate behaves.

We have focused on this model in the low-density limit. When studied in the limit of low band filling, the attractive Hubbard model represents a system with low quasi-particle densities, and therefore the weakly overlapping pairs proposed to characterize the cuprate superconductors are a natural consequence of this problem. An approximation which works well in the dilute limit is the ladder approximation; this formalism accounts for all possible scattering events for particles that can occur in the particle–particle channel (only particle–hole scatterings are ignored).

In a simple and elegant paper [8], Schmitt-Rink *et al* studied such model systems and concluded, at least in a non-self-consistent treatment of such problems, that in 2D a stable, two-particle, bound state persists down to $T = 0$, and this leads to a $T = 0$ Bose condensation of composite bosons (two fermions pair to form a boson). The physics of this phenomenon is that the appearance of preformed pairs leads to the elimination of the Fermi surface (there are no fermions left), and therefore superconductivity is suppressed in favour of $T = 0$ Bose condensation.

The consequence of this work for the model system under consideration is as follows: in a non-self-consistent treatment of the attractive Hubbard model at low densities, employing the ladder approximation, the system is always unstable towards $T = 0$ Bose condensation of preformed pairs into an infinite-lifetime, two-particle, bound state [8]. One of the focuses of this paper, and a second motivating force behind our study, is the wish to test whether this idea survives when the theory is solved in a fully self-consistent fashion. That is, when one includes interactions between pairs, does the physics of reference [8] survive? A careful and detailed study of the interaction between pairs was given by Haussmann [9, 10],

and here we will consider these ideas as applied to the observed normal-state anomalies, including the formation of a pseudo-gap, and to the physics of reference [8].

The numerical work of Haussmann for 3D suggests that the physics of this problem is very different to that of its non-self-consistent counterpart. In particular, he suggests that the bound state strongly hybridizes with the two-particle scattering continuum, and that this greatly reduces the likelihood of the appearance of preformed pairs. Such a tendency has also been suggested by the work of several other authors. Fresard and co-workers [11] found for 2D, by applying the self-consistent ladder approximation, that in the low-doping regime the Fermi-liquid properties are fully recovered and that only in the strong coupling regime can deviations from Fermi-liquid behaviour be expected. Micnas *et al* [12] found among other results that Fermi-liquid properties recover in a self-consistent calculation. (The work of these authors differs from our own work in that they use a very different method to obtain the dynamical properties of this model in this approximation.) Also, Singer *et al* [13] employed quantum Monte Carlo methods and concluded that the two-particle bound state, which they refer to as a 'band of pairs', is strongly overlapping with the one-particle continuum, and only at very large attractive interactions does it become well separated from the one-particle continuum. Lastly, recent analytical work by Kagan *et al* [14] shows that when pair–pair interactions are included in a $T = 0$ calculation, in the dilute limit the gap between the two-particle bound state and the one-particle continuum starts to close.

Our results are consistent with the above-stated trends, and we do not find that the physics of reference [8] survives when pair–pair interactions are included. Furthermore, we find no evidence of a pseudo-gap. We have used double-time Green's functions to study this system at $T > 0$, and thus, unlike in other studies that examined this system using imaginary times (the conventional Matsubara frequency formulation), in which the authors had to rely on Padé approximants or maximum-entropy techniques, we are able to examine the dynamical properties of this system directly. Thus, we believe that we have a somewhat more reliable representation of the dynamics of this system.

We organize our paper as follows. In section 2 we introduce the model and describe different levels of approximation which can be used for the ladder approximation. In the next section we introduce a $\boldsymbol{k}$-averaged method along with a generalized spectral representation of all temperature-dependent Green's functions which enables us to obtain results in a fully self-consistent calculation along the real-time axis. In section 3.2 we present numerical evidence that aids in justifying these approximations. Our main results are presented in section 4, and in section 5 we present our conclusions.

2. The model

The model Hamiltonian which we consider is the attractive (negative-U) Hubbard model, given by

$$H = -t \sum_{\langle ij\rangle,\sigma} (c^{\dagger}_{i,\sigma} c_{j,\sigma} + \mathrm{HC}) - |U| \sum_{i} n_{i,\uparrow} n_{i,\downarrow} \tag{1}$$

where t is the transfer integral connecting neighbouring lattice sites i, j, the $c^{\dagger}_{i,\sigma}$, $c_{i,\sigma}$ are electronic creation, annihilation operators, respectively, and $|U|$ is the strength of the on-site attractive interaction between two electrons occupying the same lattice site. Throughout this paper we restrict our attention to d-dimensional hypercubic lattices.

For completeness, we begin by reviewing the well studied ladder approximation to the Bethe–Salpeter equation [16, 9]. The Dyson equation which has to be solved to obtain the full one-particle Green's function contains a large number of complicated diagrams and

cannot be solved exactly. However, in the ladder approximation, which accounts for all possible scattering events for particles that can occur in the particle–particle channel (only particle–hole scatterings are ignored), one can find a solution for the single-particle self-energy. The ladder approximation can be motivated in the dilute limit by taking $k_F a$, the Fermi momentum multiplied by the scattering length (which in 3D is given by

$$a = \frac{m|U|L^3}{4\pi\hbar^2}$$

which is the effective range of the attractive potential) as an additional small parameter. This is so because all diagrams which include more than one hole propagator (crossing diagrams) are neglected, and therefore this approximation is valid in the low-density limit. The repeated scattering enters the equation through the vertex function $\Gamma(K, \mathrm{i}\Omega_n)$, and since the interaction $|U|$ is constant, the Bethe–Salpeter equation which determines $\Gamma(K, \mathrm{i}\Omega_n)$ becomes exactly solvable.

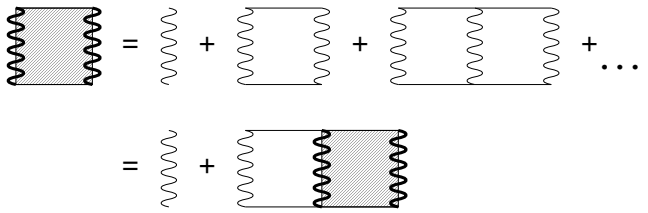

Figure 1. A diagrammatic representation of equation (3). The vertex function Γ contains the repeated scattering of two particles.

To display this solution we introduce the pair susceptibility, $\chi(\boldsymbol{K}, \mathrm{i}\Omega_n)$, given by

$$\chi(\boldsymbol{K}, \mathrm{i}\Omega_n) = -\frac{1}{N\beta}\sum_{m,\boldsymbol{k}} G(\boldsymbol{K}-\boldsymbol{k}, \mathrm{i}\Omega_n - \mathrm{i}\omega_m)G(\boldsymbol{k}, \mathrm{i}\omega_m) \tag{2}$$

where $G(\boldsymbol{k}, \mathrm{i}\omega_m)$ is the one-particle thermal Green's function. Note that the sign of this function is chosen differently by different authors, and readers should take note of the consequence of this sign choice in future equations. Then, we can express the solution for the vertex function as

$$\tilde{\Gamma}(\boldsymbol{K}, \mathrm{i}\Omega_n) = -|U|/(1 + |U|\chi(\boldsymbol{K}, \mathrm{i}\Omega_n)) \tag{3}$$

which is shown diagrammatically in figure 1.

In our work we have chosen to subtract the interaction strength from $\tilde{\Gamma}$ to obtain an analytic function $\Gamma(\boldsymbol{K}, z)$ with properties appropriate for examination by a generalized Kramers–Kroning analysis (this is equivalent to subtracting the Hartree potential from the self-energy), and thus introduce

$$\Gamma(\boldsymbol{K}, \mathrm{i}\Omega_n) = \tilde{\Gamma}(\boldsymbol{K}, \mathrm{i}\Omega_n) - (-|U|) = \frac{U^2\chi(\boldsymbol{K}, \mathrm{i}\Omega_n)}{1 + |U|\chi(\boldsymbol{K}, \mathrm{i}\Omega_n)}. \tag{4}$$

From now on, we shall only refer to Γ.

The criterion which determines a breakdown of the normal state due to superconducting pair formation with decreasing temperature is known as the Thouless criterion [17]. We have examined this condition in detail, and will report on our results elsewhere [30]. Here, we simply remark that the Thouless condition is associated with the occurrence of a two-particle bound state (with infinite lifetime) at the chemical potential, and is signified by

$$1 + |U|\chi(\boldsymbol{K} = 0, z = 0) = 0. \tag{5}$$

This equation, and the associated normal-state properties, can be examined in a variety of increasingly more accurate approximations, and we review these approximations before proceeding to our results.

2.1. Non-self-consistent, non-conserving theory

The self-energy in this case (from now on denoted by NSCNC) is given by

$$\Sigma^0(\boldsymbol{k}, \mathrm{i}\omega_n) = \frac{1}{N\beta} \sum_{m,\boldsymbol{q}} \Gamma^0(\boldsymbol{k}+\boldsymbol{q}, \mathrm{i}\omega_m + \mathrm{i}\omega_n) G^0(\boldsymbol{q}, \mathrm{i}\omega_m). \tag{6}$$

The superscript 0 indicates the use of free Green's functions. The full Green's function in this approximation is

$$G(\boldsymbol{k}, \mathrm{i}\omega_n) = G^0(\boldsymbol{k}, \mathrm{i}\omega_n) + G^0(\boldsymbol{k}, \mathrm{i}\omega_n)\Sigma^0(\boldsymbol{k}, \mathrm{i}\omega_n)G^0(\boldsymbol{k}, \mathrm{i}\omega_n). \tag{7}$$

Most importantly, Schmitt-Rink *et al* [8] have used this level of approximation and have shown that for any 2D system with an attractive interaction the system is unstable against the effective emptying of the Fermi 'circle' into the two-particle bound state. Then, a condensation at $T = 0$ of these non-interacting composite bosons takes place. While there has been some criticism of this simple and elegant idea [1], we believe that for any non-self-consistent theory the ideas of reference [8] are solid. What happens when one includes self-consistency, namely when one includes pair interactions, is one of the focuses of this paper. Furthermore, unlike the authors of reference [1], we believe that it is more appropriate to assess the credibility of the ideas of reference [8] using the same kind of formalism.

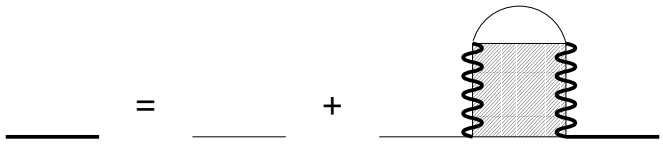

Figure 2. A diagram for the single-particle Green's function (solid line) in the non-self-consistent, conserving approximation (NSCC). The thin solid lines represent the non-interacting Green's function.

2.2. Non-self-consistent, conserving theory

We are studying a lattice model which has particle–hole symmetry. Unfortunately, the NSCNC approximation violates this symmetry. It can be restored if instead of equation (7) for the Green's function we use

$$G(\boldsymbol{k}, \mathrm{i}\omega_n) = (G^0(\boldsymbol{k}, \mathrm{i}\omega_n)^{-1} - \Sigma^0(\boldsymbol{k}, \mathrm{i}\omega_n))^{-1}. \tag{8}$$

The diagram for the full Green's function is shown in figure 2 and from now on we refer to this level of approximation as NSCC.

It was suggested by Serene [18] that the inclusion of these new diagrams fundamentally changes the physics of reference [8]. At least for the attractive Hubbard model, we do not agree with this claim, and instead find that the physics of reference [8] is still correct and, in fact, is greatly simplified when one uses a NSCC approximation.

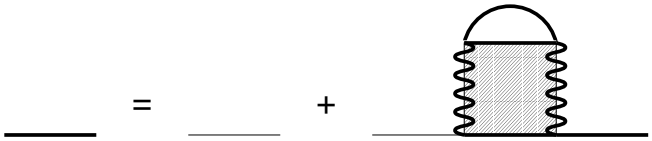

Figure 3. A diagram for the single-particle Green's function in the self-consistent, conserving (SCC) approximation, with the same notation as figures 1 and 2.

2.3. Self-consistent, conserving theory

One may treat the ladder approximation fully self-consistently by calculating the self-energy using the full interacting Green's function. That is, one solves for

$$\Sigma(\boldsymbol{k}, \mathrm{i}\omega_n) = \frac{1}{N\beta} \sum_{m,\boldsymbol{q}} \Gamma(\boldsymbol{k}+\boldsymbol{q}, \mathrm{i}\omega_m + \mathrm{i}\omega_n) G(\boldsymbol{q}, \mathrm{i}\omega_m) \tag{9}$$

$$G(\boldsymbol{k}, \mathrm{i}\omega_n) = (G^0(\boldsymbol{k}, \mathrm{i}\omega_n)^{-1} - \Sigma(\boldsymbol{k}, \mathrm{i}\omega_n))^{-1}. \tag{10}$$

Equation (10) is shown diagrammatically in figure 3, and from now on we refer to this level of approximation as SCC. (Note that we find that nothing new is learned when one examines the self-consistent, non-conserving level of approximation, and in this paper we ignore such equations.) The significant achievement of a self-consistent calculation is the inclusion of pair–pair interactions, as was stated previously by Haussmann [9]; unlike Haussmann, who studied a 3D continuous system, here we study a 2D lattice system, and are thus able to give a critique of the physics of reference [8].

Equations (2), (4), (9) and (10) have to be solved in an iterative way until self-consistency is achieved. Our procedure for accomplishing this, along the real-time axis, is discussed in the next section.

3. Calculation procedure

3.1. Formalism

In this section we outline how we solved the self-consistency problem in our $\boldsymbol{k}$-averaged approximation. Also, we have employed another approximation in the spectral representations for certain functions, and here we make this approach clear. Lastly, as was mentioned earlier, our work on this problem involves the real-frequency formulation of the thermal Green's functions. This formulation follows naturally from the analyticity of the retarded (and advanced) Green's function which is, e.g., explained in the work of Zubarev [19], and we refer the reader to this reference for further details. The work in this section makes clear the relationship between this formalism and the Matsubara frequency formalism.

In order to solve for the non-self-consistent version of the ladder approximation, in either conserving or non-conserving theories, one uses the lattice Green's function to evaluate the pair susceptibility. The susceptibility is used to calculate the vertex, from which one can evaluate the self-energy. In order to solve for these equations self-consistently, one uses the self-energy to evaluate a new approximation for the Green's function, and repeats the above process until the resulting Green's function converges.

In our $\boldsymbol{k}$-averaged approximation, we require only the momentum-averaged pair susceptibility; thus, only the momentum-averaged Green's function is required. That is,

denoting the $\boldsymbol{k}$-averaged quantities by overlined quantities:

$$\overline{\chi}(\mathrm{i}\Omega_n) \equiv \frac{1}{N}\sum_{\boldsymbol{K}} \chi(\boldsymbol{K}, \mathrm{i}\Omega_n) \tag{11}$$

or

$$\overline{\chi}(\mathrm{i}\Omega_n) = -\frac{1}{\beta}\sum_{m} \overline{G}(\mathrm{i}\Omega_n - \mathrm{i}\omega_m)\overline{G}(\mathrm{i}\omega_m). \tag{12}$$

As a computational approximation, we use a spectral representation for the $\boldsymbol{k}$-averaged functions: they are approximated by a number of δ-functions (typically several hundred) along the real axis. These δ-functions were placed in such a fashion that they are exponentially dense around the chemical potential (with a spacing $\Delta E \ll k_B T$) and around the lower band edge. The advantage of this representation is that all frequency summations appearing in our $\boldsymbol{k}$-averaged approximation can be done analytically.

According to our spectral representation, the averaged one-particle Green's function reads as follows:

$$\overline{G}^{\tilde{m}}(\mathrm{i}\omega_n) = \frac{1}{\pi}\int \frac{A(\omega)}{\mathrm{i}\omega_n - \omega}\,\mathrm{d}\omega \approx \sum_{j}^{N(\tilde{m})} \frac{a_j^{\tilde{m}}}{\mathrm{i}\omega_n - b_j^{\tilde{m}}}. \tag{13}$$

To express the Green's function in terms of a series of poles along the real axis, where to every frequency can belong a superposition of different degenerate energy levels, is usually called the Lehmann representation [20, 21]. In this way we also understand our approximation above.

The function $A(\omega)$ is the imaginary part of the (retarded) one-particle Green's function along the real axis [19, 22]. The superscript $(\tilde{m})$ in this and future quantities labels the number of the iteration step as convergence to self-consistency is performed. Furthermore, $N(\tilde{m})$ is the number of δ-functions which were used, $b_j^{\tilde{m}}$ is the position of each δ-peak on the real axis, and $a_j^{\tilde{m}}$ is the weight of this peak.

If we define the averaged Green's function in this way, we can calculate analytically the frequency summation which is needed to obtain the averaged pair susceptibility $\overline{\chi}^{\tilde{m}}(\mathrm{i}\Omega_n)$:

$$\begin{aligned}
\overline{\chi}^{\tilde{m}}(\mathrm{i}\Omega_n) &= -\sum_{j,k}^{N(\tilde{m})} \frac{1}{\beta}\sum_{m} \frac{a_j^{\tilde{m}}}{\mathrm{i}\omega_m - b_j^{\tilde{m}}} \frac{a_k^{\tilde{m}}}{\mathrm{i}\Omega_n - \mathrm{i}\omega_m - b_k^{\tilde{m}}} \\
&= \sum_{j,k}^{N(\tilde{m})} \frac{a_j^{\tilde{m}} a_k^{\tilde{m}}}{\mathrm{i}\Omega_n - b_j^{\tilde{m}} - b_k^{\tilde{m}}}\left(\frac{1}{1+\mathrm{e}^{+\beta b_j^{\tilde{m}}}} - \frac{1}{1+\mathrm{e}^{-\beta b_k^{\tilde{m}}}}\right) \\
&= \frac{1}{2}\sum_{j,k}^{N(\tilde{m})} \frac{a_j^{\tilde{m}} a_k^{\tilde{m}}}{\mathrm{i}\Omega_n - b_j^{\tilde{m}} - b_k^{\tilde{m}}}\left(\tanh\left(\frac{\beta b_j^{\tilde{m}}}{2}\right) + \tanh\left(\frac{\beta b_k^{\tilde{m}}}{2}\right)\right)
\end{aligned} \tag{14}$$

which can be abbreviated as

$$\overline{\chi}^{\tilde{m}}(\mathrm{i}\Omega_n) = \sum_{k}^{M(\tilde{m})} \frac{c_k^{\tilde{m}}}{\mathrm{i}\Omega_n - d_k^{\tilde{m}}} \tag{15}$$

and hence has an identical formal structure to the $\boldsymbol{k}$-averaged Green's function in our spectral representation, but the spectral weights of the poles are now given by $c_k^{\tilde{m}}$ at positions $d_k^{\tilde{m}}$ along the real axis. Here

$$M(\tilde{m}) = \frac{N(\tilde{m})(N(\tilde{m})+1)}{2}$$

is the new number of poles that are included in the representation for the pair susceptibility.

With $\overline{\chi}^{\tilde{m}}(\mathrm{i}\Omega_n)$ we can now calculate $\overline{\Gamma}^{\tilde{m}}(\mathrm{i}\Omega_n)$, which in our theory is given by

$$\overline{\Gamma}(\mathrm{i}\Omega_n) = \frac{1}{N}\sum_{\boldsymbol{K}}\Gamma(\boldsymbol{K},\mathrm{i}\Omega_n) \approx \frac{U^2\overline{\chi}(\mathrm{i}\Omega_n)}{(1+|U|\overline{\chi}(\mathrm{i}\Omega_n))}\left[1+\frac{U(\overline{\chi}^2-\overline{\chi^2})}{\overline{\chi}(1+|U|\overline{\chi})}+\cdots\right]. \tag{16}$$

We assume that the second term in the expansion, proportional to the mean squared fluctuations of the pair susceptibility, and higher-order terms, can be neglected on the basis of our knowledge that they should tend to zero in infinite spatial dimensions. In order to obtain a spectral representation for Γ we use partial fractions:

$$\begin{aligned}\overline{\Gamma}^{\tilde{m}}(\mathrm{i}\Omega_n) &= \frac{U^2\overline{\chi}^{\tilde{m}}(\mathrm{i}\Omega_n)}{1-U\overline{\chi}^{\tilde{m}}(\mathrm{i}\Omega_n)} \\ &= \left(U^2\sum_k^{M(\tilde{m})} c_k^{\tilde{m}}\prod_{l\neq k}(\mathrm{i}\Omega_m - d_l^{\tilde{m}})\right) \\ &\quad\times\left(\prod_k(\mathrm{i}\Omega_m-d_k^{\tilde{m}}) - U\sum_k^{M(\tilde{m})} c_k^{\tilde{m}}\prod_{l\neq k}(\mathrm{i}\Omega_m-d_l^{\tilde{m}})\right)^{-1} \\ &= \sum_m^{M(\tilde{m})}\frac{g_m^{\tilde{m}}}{\mathrm{i}\Omega_n - h_m^{\tilde{m}}}.\end{aligned} \tag{17}$$

The position of the poles $h_m^{\tilde{m}}$ along the real axis is given by the zeros of the polynomial

$$\prod_k(x-d_k^{\tilde{m}}) - U\sum_k^{M(\tilde{m})} c_k^{\tilde{m}}\prod_{l\neq k}(x-d_l^{\tilde{m}}) = 0 \tag{18}$$

which have to be determined numerically. The weight factors $g_m^{\tilde{m}}$ follow from the equation

$$g_m^{\tilde{m}} = U^2\sum_k^{M(\tilde{m})} c_k^{\tilde{m}}\prod_{l\neq k}(h_m^{\tilde{m}} - d_l^{\tilde{m}}). \tag{19}$$

With the result for Γ, we obtain an equation for the spectral representation of Σ:

$$\begin{aligned}\overline{\Sigma}^{\tilde{m}}(\mathrm{i}\omega_n) &= \sum_r^{M(\tilde{m})}\sum_s^{N(\tilde{m})}\frac{1}{\beta}\sum_m\frac{g_r^{\tilde{m}}}{\mathrm{i}\omega_n+\mathrm{i}\omega_m-h_r^{\tilde{m}}}\frac{a_s^{\tilde{m}}}{\mathrm{i}\omega_m-b_s^{\tilde{m}}} \\ &= \sum_r^{M(\tilde{m})}\sum_s^{N(\tilde{m})}\frac{g_r^{\tilde{m}}a_s^{\tilde{m}}}{\mathrm{i}\omega_n-h_r^{\tilde{m}}+b_s^{\tilde{m}}}\left(\frac{1}{1+\mathrm{e}^{\beta b_s^{\tilde{m}}}}-\frac{1}{1-\mathrm{e}^{\beta h_r^{\tilde{m}}}}\right).\end{aligned} \tag{20}$$

Again we can abbreviate this as

$$\overline{\Sigma}^{\tilde{m}}(\mathrm{i}\omega_n) = \sum_t^{N(\tilde{m})M(\tilde{m})}\frac{s_t^{\tilde{m}}}{\mathrm{i}\omega_n - t_t^{\tilde{m}}}. \tag{21}$$

To determine the equation for G in the next level of iteration we use partial fractions again:

$$\begin{aligned}\overline{G}^{n+1}(\mathrm{i}\omega_n) &= \sum_j^{N(0)}\frac{a_j^0}{\mathrm{i}\omega_n - b_j^0 - \overline{\Sigma}^{\tilde{m}}(\mathrm{i}\omega_n)} = \sum_i^{N(0)}\left[\left(a_i^0\prod_t(\mathrm{i}\omega_n - t_t^{\tilde{m}})\right)\Big/(C(\mathrm{i}\omega_n)-D(\mathrm{i}\omega_n))\right] \\ &= \sum_i^{N(\tilde{m}+1)}\frac{a_i^{n+1}}{\mathrm{i}\omega_n - b_i^{n+1}}\end{aligned} \tag{22}$$

where we used the abbreviations

$$C(\mathrm{i}\omega_n) = (\mathrm{i}\omega_n - b_j^0)\prod_t(\mathrm{i}\omega_n - t_t^{\tilde{m}})$$
$$D(\mathrm{i}\omega_n) = \sum_t^{N(\tilde{m})M(\tilde{m})} s_t^{\tilde{m}} \prod_{u\neq t}(\mathrm{i}\omega_n - t_u^{\tilde{m}}). \tag{23}$$

The poles b_j^{n+1} for the spectral representation of $\overline{G}^{n+1}(\mathrm{i}\omega_n)$ are given by the zeros of the polynomial

$$(\mathrm{i}\omega_n - b_j^0)\prod_t(\mathrm{i}\omega_n - t_t^{\tilde{m}}) - \sum_t^{N(\tilde{m})M(\tilde{m})} s_t^{\tilde{m}} \prod_{u\neq t}(\mathrm{i}\omega_n - t_u^{\tilde{m}}) = 0 \tag{24}$$

and the weight factors a_j^{n+1} are obtained by inserting the results for the poles in equation (22).

By going through one loop of self-consistency in this equation, the number of poles is increased from $N(\tilde{m})$ to

$$N(0)N(\tilde{m})M(\tilde{m}) = N(0)N(\tilde{m})^2(N(\tilde{m})+1)/2.$$

To avoid the number of δ-functions that we have to deal with exceeding the number that we can handle numerically and to avoid divergences which can occur if two poles come too close to each other, we apply two additional approximations. First, we unite two delta peaks to a single one if their positions come closer to each other than $\epsilon(\omega)$, where ϵ is smallest at the chemical potential and at the lower band edge of the unperturbed system. Second, we neglect a pole whose weight is smaller than a certain boundary $\nu(\omega)$ which is again smallest at the chemical potential. This has to be done in such a way that the loss of spectral weight is distributed onto all other poles in order to fulfil the sum rules.

In this way we have solved equation (14) to equation (24) until a stable self-consistent solution is obtained. $N(0)$ is typically chosen to be around 20, and we end up with $N(\tilde{m}_{max})$ of the order of 300 and at no step of the calculation does the number of poles exceed 3000.

We can therefore do the whole self-consistency loop by calculating all quantities *along the real axis*. In order to show that this is indeed equivalent to the imaginary-axis Matsubara frequency formalism, we show how one can calculate the particle number in both formalisms. The expectation value of the particle number, $\langle n\rangle$, can be calculated either by summing over the poles along the imaginary axis or by summing over the δ-functions along the real axis:

$$\langle n\rangle = \frac{1}{\beta}\sum_{\ell=-\infty}^{\infty} G(\mathrm{i}\omega_\ell) = 1 + \frac{2}{\beta}\sum_{\ell=0}^{\infty}\mathrm{Re}(G(\mathrm{i}\omega_\ell)) \tag{25}$$

which can be expressed by using the spectral representation as an integration along the real axis:

$$\begin{aligned}\langle n\rangle &= \lim_{\delta\to 0^+}\frac{1}{2\pi\mathrm{i}}\oint \frac{\mathrm{e}^{\mathrm{i}\delta}}{1+\mathrm{e}^{\beta z}}G(z)\,\mathrm{d}z \\ &= \lim_{\delta\to 0^+}\frac{1}{2\pi\mathrm{i}}\oint \frac{\mathrm{e}^{\mathrm{i}\delta}}{1+\mathrm{e}^{\beta z}}\frac{1}{\pi}\int_{-\infty}^{\infty}\frac{A(x)}{z-x}\,\mathrm{d}x\,\mathrm{d}z \\ &= \frac{1}{\pi}\int_{-\infty}^{\infty}\frac{A(x)}{1+\mathrm{e}^{\beta x}}\,\mathrm{d}x.\end{aligned} \tag{26}$$

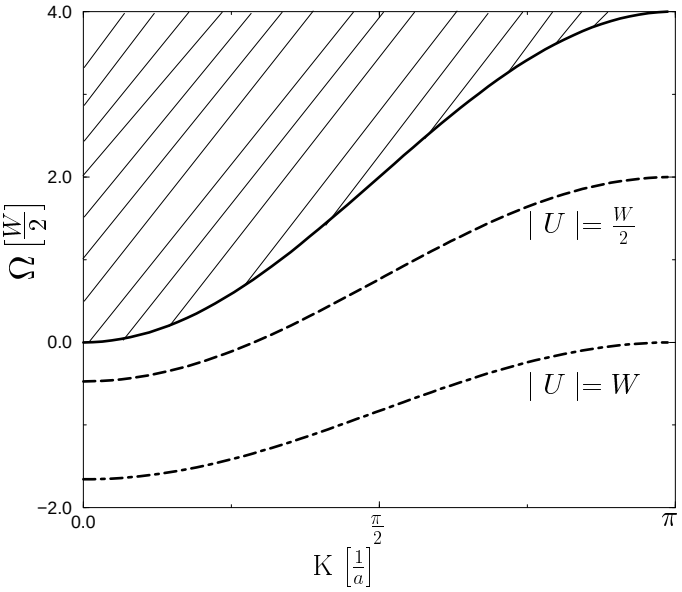

Figure 4. A schematic diagram of the dispersion of the two-particle bound state below the non-interacting continuum of the susceptibility $\chi(K, \Omega)$ (shaded region) as it arises in a NSC formulation, if the chemical potential is below the continuum. The k-average approximation is related to ignoring the dispersion of this band of states.

This can be reduced by approximating the spectral function as a sum of δ-functions as was done above:

$$A(x) \approx \sum_{j}^{N(\tilde{m})} a_j^{\tilde{m}} \pi \delta(x - b_j^{\tilde{m}}). \tag{27}$$

Altogether, we can express the particle number with these δ-functions:

$$\langle n \rangle \approx \frac{1}{\pi} \int_{-\infty}^{\infty} \frac{1}{1 + \mathrm{e}^{\beta x}} \sum_{j}^{N(\tilde{m})} a_j^{\tilde{m}} \pi \delta(x - b_j^{\tilde{m}}) \, \mathrm{d}x = \sum_{j}^{N(\tilde{m})} \frac{a_j^{\tilde{m}}}{1 + \mathrm{e}^{\beta b_j^{\tilde{m}}}}. \tag{28}$$

Note that the dimensionality of the system enters into this calculation as the shape of G^0, whose imaginary part is the spectral function of the uncorrelated system. To obtain numerical results we constructed the unperturbed Green function G^0 from a number (typically 20) of δ-functions. Since the most important physics is happening at the chemical potential and at the lower band edge, we choose the distance between the δ-peaks to be smallest at these points. To make sure that the distance between two δ-peaks is always smaller than $k_B T$, at these points we made these distances exponentially small by sampling the points with a $\tanh^{-1}(\beta x)$ function around the chemical potential and around the lower band edge.

3.2. Justification of the $\boldsymbol{k}$*-averaged method*

In the following we discuss limiting cases where the $\boldsymbol{k}$-average approximation made in equation (16) becomes manifestly justifiable.

This is the case for large temperatures since $1 - \langle n_{\boldsymbol{K}/2+\boldsymbol{q}} \rangle - \langle n_{\boldsymbol{K}/2-\boldsymbol{q}} \rangle$, as the numerator for the calculation of χ, is small. Therefore χ becomes small. Of course, this is simply the

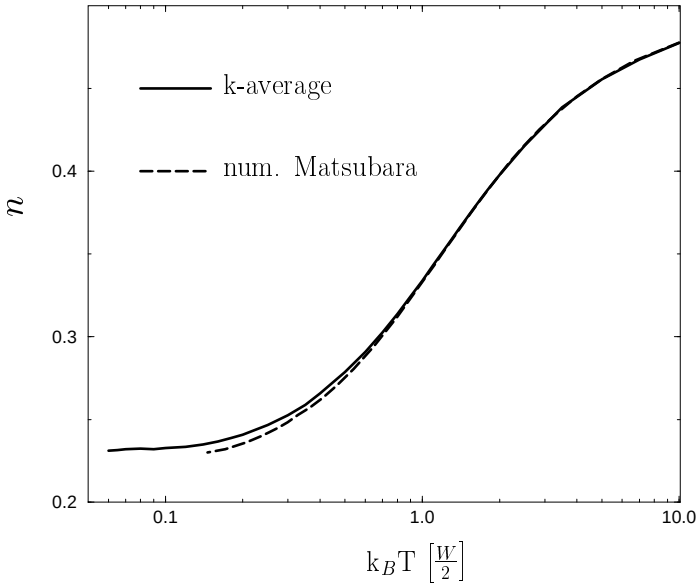

Figure 5. For a fixed chemical potential ($\mu = -0.9$) the particle number is plotted as a function of the temperature. All of the quantities are measured in units of half the bandwidth, $W = 4t$ for 1D, and a value of $|U| = W$ is used. The k-average method is compared with a numerical summation on a finite lattice (60 sites) and for a finite number of Matsubara frequencies (150). The two methods give essentially the same result. Note the logarithmic temperature scale.

uncorrelated limit (note that a $\boldsymbol{k}$-dependence still survives in the Green's function, since the free Green's function has such a dependence). The approximation also holds true trivially for small bandwidth and becomes exact if the band can be approximated by a δ-function (namely, in the atomic limit, for which $t \longrightarrow 0$). In this case no $\boldsymbol{k}$-dispersion is present in the problem. Furthermore, the case with $|U| = 0$ is trivially correct.

For $|U|$ not too large, Γ is determined by the pole of the bound state at $\chi = 1/|U|$, which means that a weakly dispersive two-particle bound state is well separated from the continuum. The dispersion becomes weaker for larger $|U|$ since the effective transfer of a pair is $t_{eff} \sim t^2/U$. So, in this case the average over $\boldsymbol{k}$-space is also a good approximation, since all we are doing is replacing the bound state below the continuum by its average. This is shown schematically in figure 4.

Probably the most interesting limit is that of large spatial dimensions. It was argued by Metzner and Vollhardt [15] that for a system with large dimensions the $\boldsymbol{k}$-dispersion of the self-energy vanishes, which in the end is very similar to what we do. Such an approximation gives several results which are seemingly also valid in 2D and 3D; for a review, see [23].

The only case where we can carefully give a critique of the quality of our fully self-consistent results found using our k-averaged method is that of a 1D model system. Of course, as we argued in relation to equation (16), in one dimension our results should be least accurate due to large fluctuation effects. Therefore, such a comparison should be viewed as an upper bound of the potential differences, and our method should work much better in any higher dimension.

In the 1D case we can directly compare results obtained by our k-averaged method (we started with a density of states $A^0(\omega) = 1/(\pi\sqrt{4t^2 - \omega^2})$ and 20 initial δ-functions) with fully self-consistent calculations (obtained by summing over the Matsubara frequencies—

we used 40 to 60 lattice points and 150 fermionic and 299 bosonic Matsubara frequencies). Of course, for the latter calculation, in order to perform this comparison, we must restrict consideration to and calculate quantities that are averaged over the Brillouin zone.

In figure 5 we have plotted the particle number as a function of the temperature for a fixed chemical potential obtained from the fully self-consistent calculations. This was done for the two entirely different calculational procedures. As one can see in this figure, we had to use a logarithmic scale to show the differences between these two results. One curve is obtained by applying the k-averaged method while the other curve is obtained taking into account the full k-dispersion and summing numerically over the Matsubara frequencies. The two methods describe the same physics, which is different from the results obtained from NSC calculations. That these curves agree so well, and the fact that we are able to use our k-averaged method to such low temperatures, is very encouraging.

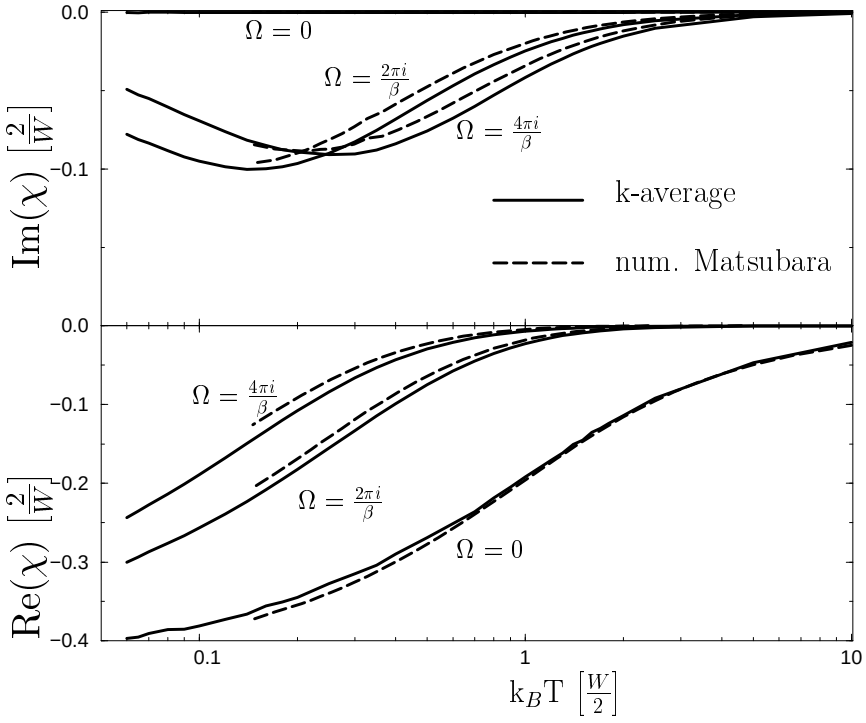

Figure 6. For three Matsubara frequencies ($\{0, 2\pi/\beta, 4\pi/\beta\}$) and for the same 1D system the susceptibility $\overline{\chi}$ is compared as a function of temperature. The two different approximations, the full-k-dependence numerical sum over Matsubara frequencies and the k-averaged method, are compared. In the upper graph the imaginary part of $\overline{\chi}$ is shown and in the lower graph the real part is shown.

We compared k-averaged susceptibilities for three Matsubara frequencies, $\Omega_n \in \{0, 2\pi\mathrm{i}/\beta, 4\pi\mathrm{i}/\beta\}$. The results in figure 6 are obtained with the k-averaged method—note that the analyticity of $\chi(z)$ allows us to evaluate also the results for the k-averaged method for imaginary frequencies. The curves in figure 6 are obtained by calculating all quantities by summing over (intermediate) Matsubara frequencies and by considering the full k-dispersion throughout the entire self-consistency calculation; then, the k-averaging is done at the very end of the calculation, after self-consistency had been established. The

temperature dependence of these susceptibility quantities shows an excellent agreement for these two completely different calculation methods. Thus, the validity of both the k-average method, and of the approximation discussed in equation (16), is demonstrated, and our method successfully reproduces the fully self-consistent calculation even in 1D, where the fluctuations in equation (16) are expected to be at their largest.

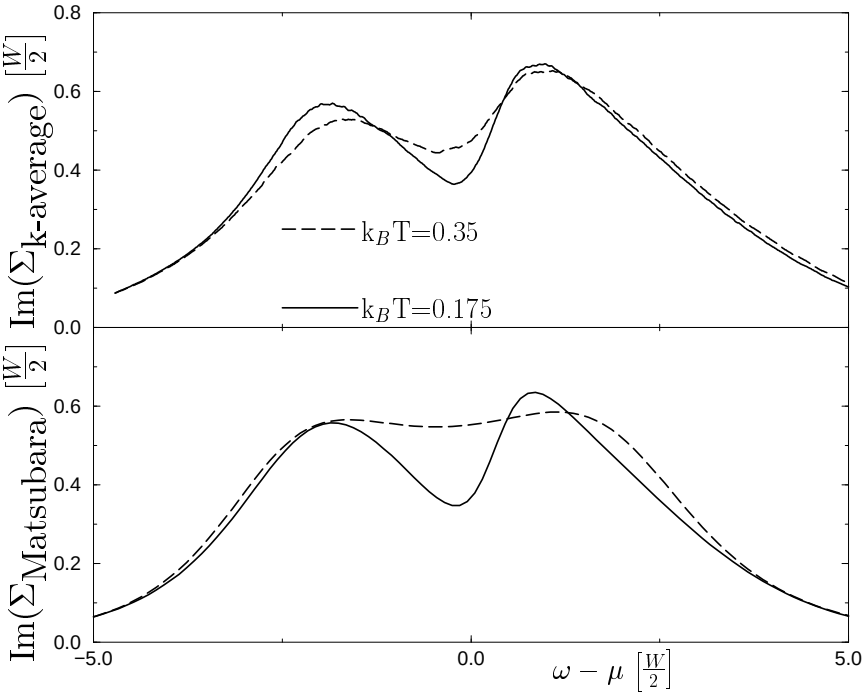

Figure 7. The k-averaged imaginary part of $\mathrm{Im}(\Sigma(\omega-\mu))$ for a 1D system is plotted. In the upper graph the k-averaged method is used whereas in the lower graph a numerical summation over Matsubara frequencies (150 points) and 60 k-points is performed with a k-average applied at the very end of the calculation. In the latter case, Padé approximants were used to obtain real-axis results. The difference at $k_BT = 0.35$ is due to the failure of the Padé approximant at sparse Matsubara frequencies. The minimum of $\mathrm{Im}(\Sigma(\omega-\mu))$ is clearly resolved in both cases for low temperatures.

To give a critique of the predictions for dynamical quantities produced by the k-averaged method, in figure 7 we compare, for two different temperatures, the imaginary parts of the k-averaged self-energy obtained (in figure 7 (upper graph)) by using the k-averaged method, and (in figure 7 (lower graph)) by applying Padé approximants, as explained in reference [25], for Matsubara frequencies where the full k-dependence has been considered. In a similar fashion we compare in figure 8 the results for the one-particle density of states. Again, the k-averaging for the Matsubara frequency method was done at the end of the fully self-consistent calculation, while the k-averaged method uses k-averaged quantities only throughout its approach to self-consistency. In both of these figures we find good agreement between the two methods, showing that the more conventional Matsubara frequency method results are reproduced by our k-averaged approach to the pair susceptibility.

Encouraged by these successes of our k-averaged method in 1D, below we consider the system of greater interest, two dimensions. Of course, although the above results are

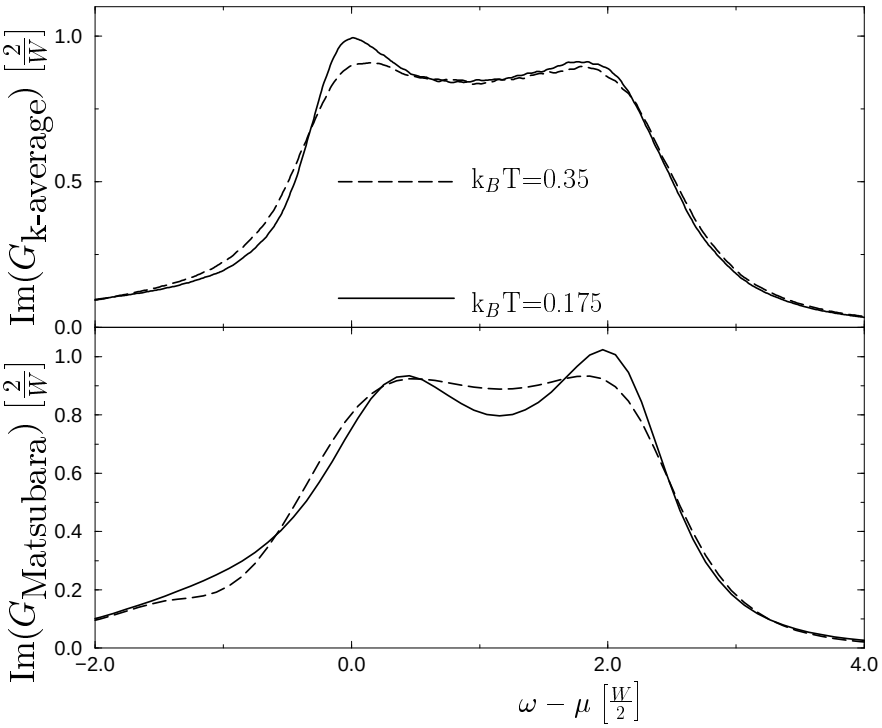

Figure 8. The 1D density of states for the two different approximations is plotted for the same temperatures as in figure 7. Note the local maximum at the chemical potential.

encouraging, we cannot claim that our method can examine all of the features of this rich system. For example, some features, like the eta mode discussed by Zhang and co-workers [26], or any other k-specific excitation, are masked by our k-averaging.

4. Results

In this section we discuss our numerical results obtained using the method described above. We focus on a quasi-2D system by starting the k-averaged calculation with a $\overline{G^0}(\omega)$ that corresponds to a constant density of states. The band fillings are chosen to be below half-filling ($n = 0.5$ is half-filling), and therefore the absence of the van Hove singularity in the middle of our 'band' is unimportant. We choose constant particle numbers ($n = 0.1$ and $n = 0.3$) and calculate the chemical potentials as a function of the temperature.

4.1. The single-particle density of states—no pseudo-gap

Of prime interest in our study is the single-particle density of states, since the presence of a pseudo-gap should be apparent in this quantity [24]. Fortunately, this is a k-averaged quantity, and so it follows immediately from the imaginary part of the self-consistent (k-averaged) single-particle Green's function.

Our results for $n = 0.1$ as a function of temperature (and which implicitly include the temperature-dependent chemical potential) are shown in figure 9. For comparison, we also show the NSCC result for one temperature. To aid in the understanding of these results, we

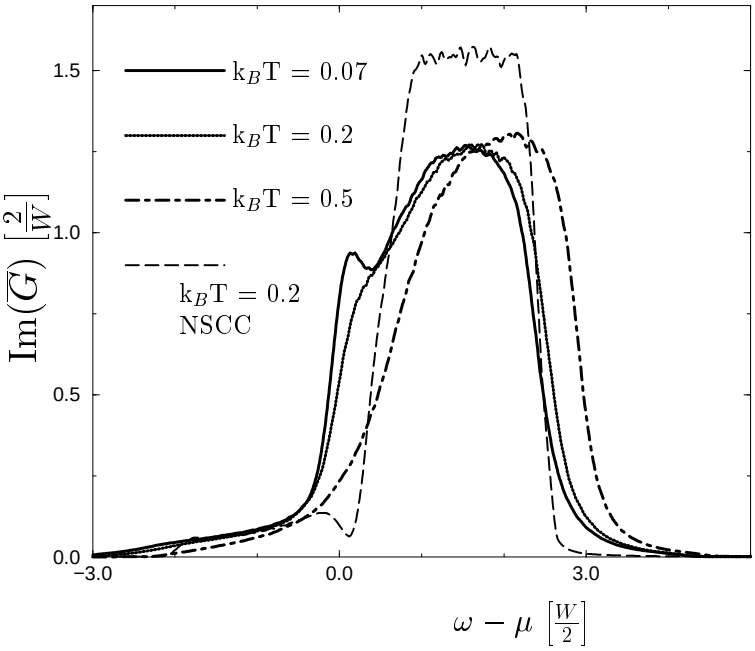

Figure 9. The resulting self-consistent density of states for the quasi-two-dimensional system with $n = 0.1$ and $|U| = 2$ for four different temperatures is shown. Note that the density of states develops a maximum at the chemical potential when the temperature is decreased. For comparison we have shown the density of states from the NSCC approximation for $k_BT = 0.2$. All energies are given in units of $W/2$.

show the behaviour of the chemical potential as a function of temperature in figure 10—this latter quantity will be discussed in considerable detail in the next subsection of the paper.

The NSCC result (which is very similar to the NSCNC result) at $k_BT = 0.2$ shows that the entire single-particle band is above the chemical potential (seen from roughly $k_BT = 0.5$ to $k_BT = 2.5$), and that below the chemical potential one finds the effects of the two-particle bound state. We stress that the 'gap' between these two features is entirely different from that found by Janko *et al* (which they proposed to be a pseudo-gap) [27], in that they study a 3D system which, more importantly, has the chemical potential inside the one-particle band. As is seen in our figure 10, for our NSCC calculation at $n = 0.1$ the chemical potential is below the continuum arising from the single-particle states. Thus, the gap feature seen in our figure near $\omega = \mu$ is not related to a pseudo-gap. Instead, we believe that this behaviour is related to the analytical work for the NSC theory described in reference [14]. Furthermore, the NSC theory provides us with an energy scale for the binding energy of the pairs, and is given by the distance of the $T = 0$ chemical potential from the lower band edge. This is, in our example ($U = W$), the density-independent number 0.31 (in units of $W/2$) or 0.19 [$W/2$] for the calculations taking into account the full k-dispersion or the k-average, respectively.

Most importantly, the fully SCC result shows no evidence of a pseudo-gap. In fact, we see the opposite of a pseudo-gap, wherein there is an increase in spectral weight at the chemical potential. Unfortunately, it is somewhat difficult to say what happens to the chemical potential for this density—so, we now consider higher densities to clarify this situation.

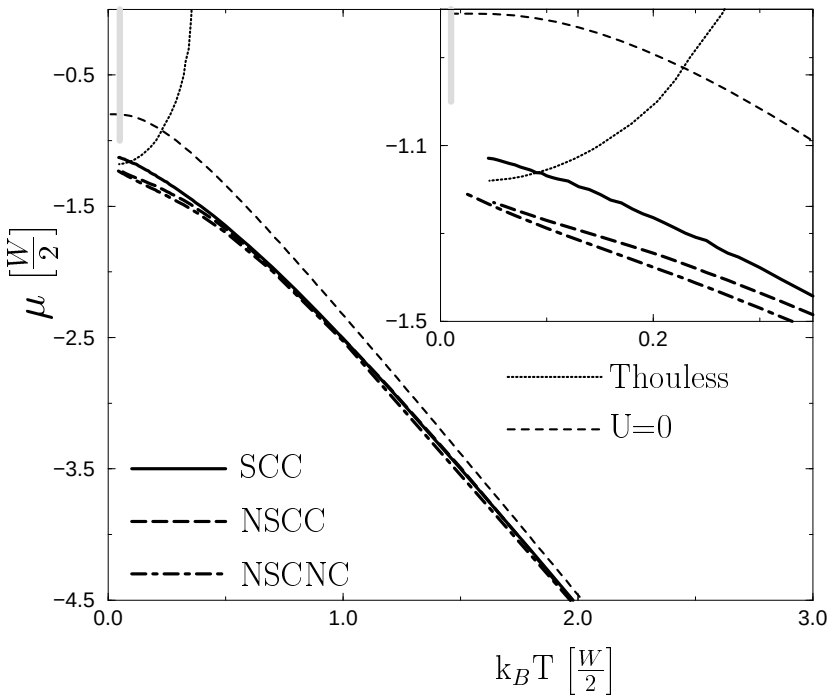

Figure 10. A flow diagram of the quasi-2D system ($n = 0.1$) for the chemical potential μ as a function of the temperature. The different levels of approximation are shown. For comparison, the line for the non-interacting system ($U = 0$) is given, and the Thouless line which determines the NSC T_c is shown. The region of the one-particle continuum of a non-interacting reference system is shown, beginning at $\mu = -1$ on the μ-axis. The parameters were chosen to be $|U| = 2$ and $n = 0.1$ and all energies are given in units of half the bandwidth, $W/2$.

Figures 11 and 12 show the analogous results for $n = 0.3$. Here, the NSCC result is similar to the above NSCC data, only now the feature from the two-particle bound state is much more clearly resolved. Also, the physics in the SCC result is more easily seen. These figures show quite clearly that (i) the chemical potential is in the band (for the SCC formulation, this is true for temperatures below about 0.9), and (ii) no evidence of a pseudo-gap is found. Instead, as above, there is an enhancement of the spectral weight near the chemical potential. This finding is in disagreement with other SCC results for a d-wave pairing potential [28].

We note that recent Monte Carlo results in the $d \longrightarrow \infty$ limit, which were obtained at $n = 0.3$ and for the same intermediate coupling that we used, also did not find a pseudo-gap [29].

4.2. Suppression of superconductivity in 2D

As mentioned in the introduction, a simple explanation of the (potential) suppression of superconductivity in 2D was given in reference [8]. The physics can be related to the behaviour of the chemical potential—namely, when an attractive potential of any strength is present in 2D (or 1D), a bound state is formed, and this state 'attracts' the chemical potential to it. Thus, the chemical potential is found below the bottom of the band, and no Fermi surface is left. No Fermi surface means that there is no Cooper pairing.

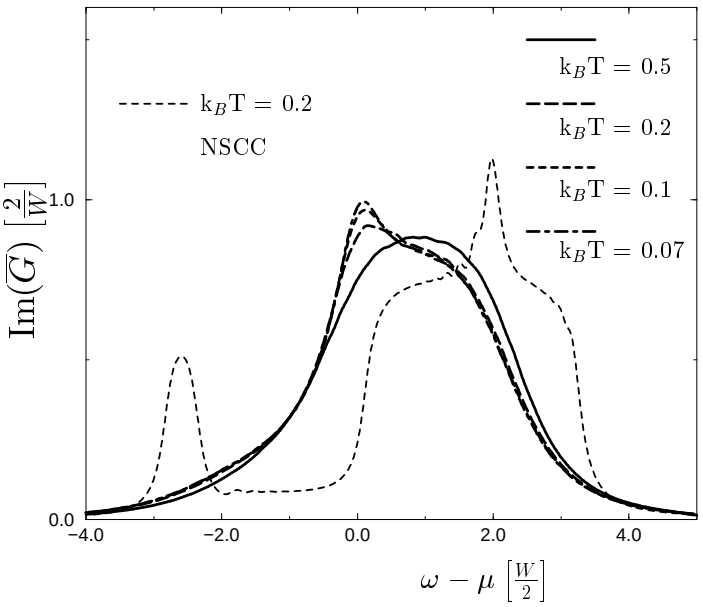

Figure 11. The same plot as in figure 9, but for a density of $n = 0.3$.

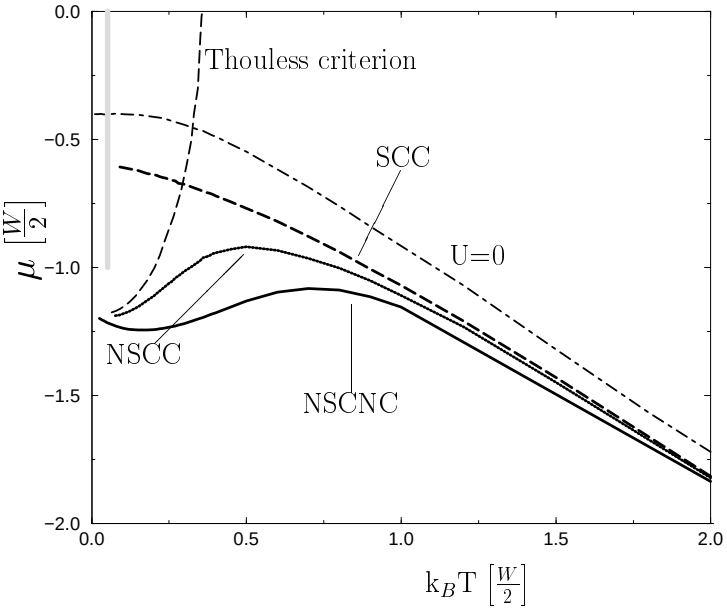

Figure 12. As figure 10, but for a density of $n = 0.3$.

We note that the formulation of reference [8] is NSCNC. Although Serene [18] has claimed that the physics of reference [8] is destroyed when one uses a conserving theory, we disagree with this. In fact, for lattice systems, we have been able to formally show that the physics of reference [8] survives, and in fact becomes more transparent, in a conserving

theory. We will discuss these results in a future publication [30].

In contrast to this, our data for the chemical potential in a SCC theory show that the physics of reference [8] does not survive the inclusion of pair–pair interactions in a fully self-consistent theory. This is easiest to see in figure 12, wherein the low-temperature extrapolation of the chemical potential is into the (interacting) single-particle band. Put another way, there is still a Fermi surface at low temperatures in a SCC theory. (That is not necessarily to say that this is a Fermi liquid—see the next subsection.) We note that the reappearance of the Fermi surface was also seen in the SCC work of Fresard and co-workers [11].

To better understand this, we now consider the behaviour of this bound state via the SCC vertex function. Examining the vertex function $\overline{\Gamma}(\Omega)$ probably best explains the difference in physics between the NSCC and the SCC formulations. For the NSCC calculation, the infinite-lifetime bound state is seen as a (numerically broadened) delta function in $\mathrm{Im}(\overline{\Gamma}(\Omega))$ (see the inset in figure 13). However, $\mathrm{Im}(\overline{\Gamma}(\Omega))$ for the SCC calculation does not show a delta peak below the continuum—instead, at the chemical potential, with decreasing temperature an enhancement near μ can be seen. Note that in figure 13 for Ω below the chemical potential there is a non-vanishing imaginary part of $\overline{\Gamma}(\Omega)$ that is negative. Therefore, the enhancement of $\mathrm{Im}(\overline{\Gamma}(\Omega))$ can also be interpreted as a lifetime-broadened remnant of a two-particle bound state. So, we stress again that for the SCC calculation there is no infinite-lifetime bound state, opposite to the case for the NSCC calculation. When treating the system self-consistently, pair–pair interactions are included which lead to a finite lifetime of the pairs, and therefore the condensation of the fermions into a bound state is hindered.

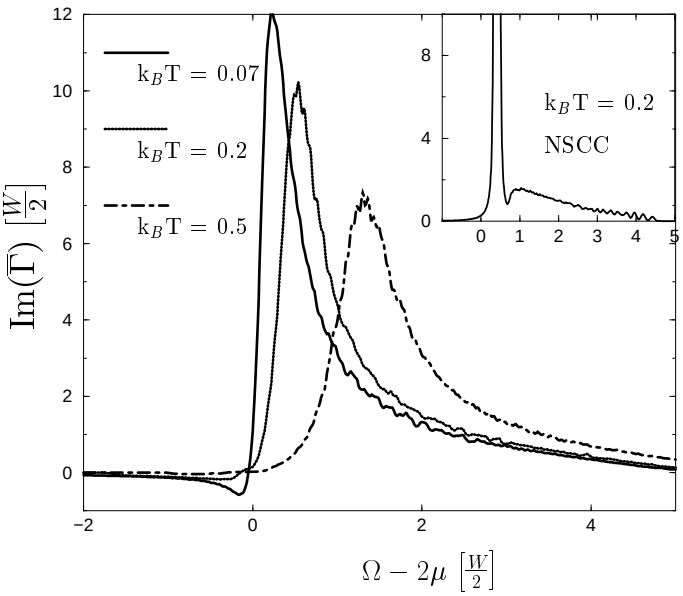

Figure 13. A plot of $\mathrm{Im}(\overline{\Gamma}(\Omega - 2\mu))$ for the quasi-2D system. The inset shows the result for $kT = 0.2$ from the NSCC calculation with a delta peak indicating the infinite-lifetime bound state. The SCC result is plotted for three temperatures (0.5, 0.2, 0.07) and shows no infinite-lifetime bound state. All of the energies are again in units of $W/2$ with $|U| = 2$ and $n = 0.1$.

4.3. The quasi-particle lifetime at the chemical potential

The above results showed that in a SCC theory the Fermi surface survives at low temperatures. The natural question is then: is this a Fermi liquid?

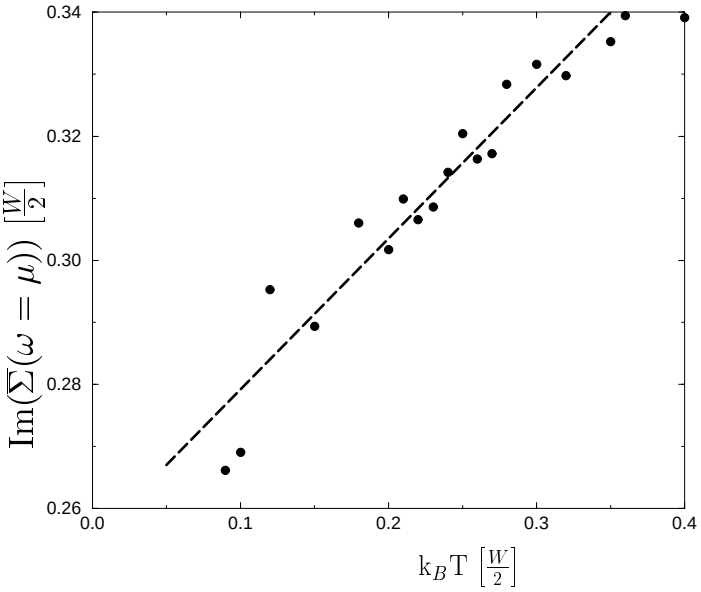

Figure 14. The imaginary part of the self-energy at the chemical potential as a function of temperature for the model parameters $|U| = 2$ and $n = 0.1$. The straight line is a guide to the eye.

To help us answer this question, we consider the (real-) frequency dependence of the imaginary part of the self-energy Σ. In a SCC theory it exhibits a minimum at the chemical potential, and this qualitative behaviour is indeed similar to that of a Fermi liquid. However, in figure 14 we have plotted this quantity, which is related to the inverse quasi-particle lifetime at the chemical potential, as a function of temperature. The calculated value seems to indicate a linear variation with temperature (the extrapolated value is simply a function of our numerical broadening, and in this calculation has no physical significance).

To understand this we note that standard arguments, based on, for example, Fermi's golden rule, predict the T^2-behaviour of a Fermi liquid. However, we argue that if the dominant scattering is between lifetime-broadened two-particle bound states and quasi-particles, then such a linear T-behaviour is indeed expected. Crucial to this argument is the approximate temperature independence of the lifetime of the two-particle bound state, something that our numerics makes clear. Furthermore, consequences of this simple phenomenology are currently being explored.

5. Conclusions

We have examined the attractive Hubbard model in 2D using a $\boldsymbol{k}$-averaged method. Furthermore, we have studied the dynamical properties of this model using real-time-axis thermal Green's functions—this allows for an accurate determination of quantities like the single-particle density of states, and the energy dependencies of the self-energy and vertex

function. We have compared our approach to the more familiar Matsubara frequency method in 1D, and have found little difference between the results obtained by the two methods. However, the $\boldsymbol{k}$-averaged method allows us to reach much lower temperatures without enormous computational efforts.

We have included pair–pair interactions, as formulated by Haussmann, in a SCC theory. Our results for such a theory lead us to believe that the attractive Hubbard model in 2D, for a correlation energy roughly equal to the bandwidth, does not have a pseudo-gap. Instead, there is actually an enhancement of the spectral weight near the Fermi surface. The nature of the ground-state properties is uncertain, since we find a linear temperature dependence of the quasi-particle scattering rate over a wide temperature range. The reappearance of the Fermi surface in a SCC theory in 2D was noted previously by Fresard and co-workers [11], but the linear T-behaviour is new, and deserves further investigation.

Acknowledgments

We wish to thank R Haussmann, B Janko, M Kagan, S Kehrrein, P Kornilovitch, A Nazarenko, M Randeria, M Ulmke, and especially F Marsiglio and A Chernyshev for helpful discussions. This work was supported by the Deutsche Forschungsgemeinschaft and by the NSERC of Canada.

References

[1] Randeria M 1995 *Bose–Einstein Condensation* ed A Griffin *et al* (Cambridge: Cambridge University Press) and references therein
[2] Warren W W, Walstedt R E, Brennert G F, Cava R J, Tycko R, Bell R F and Dabbagh G 1989 *Phys. Rev. Lett.* **62** 1193
[3] Takigawa M, Reyes A P, Hammel P C, Thompson J D, Heffner R H, Fisk Z and Ott K C 1991 *Phys. Rev.* B **43**
[4] Alloul H, Mahajan A, Casalta H and Klein O 1993 *Phys. Rev. Lett.* **70** 1171
[5] Puchkov A V, Fournier P, Basov D N, Timusk T, Kapitulnik A and Kolesnikov N N 1996 *Phys. Rev. Lett.* **77** 3212
[6] Puchkov A, Basov D and Timusk T 1996 *J. Phys.: Condens. Matter* **8** 10 049
[7] Fischer O 1997 *SNS1997 (Cape Cod, MA)* talk
[8] Schmitt-Rink S, Varma C M and Ruckenstein A E 1989 *Phys. Rev. Lett.* **63** 445
[9] Haussmann R 1993 *Z. Phys.* B **91** 291
[10] Haussmann R 1994 *Phys. Rev.* B **49** 12 975
[11] Wölfle P, Fresard R and Glaser B 1992 *J. Phys.: Condens. Matter* **4** 8565
[12] Micnas R, Pedersen M H, Schafroth S, Schneider T, Rodriguez-Nunez J J and Beck H 1995 *Phys. Rev.* B **52** 16 223
[13] Singer J M, Pedersen M H, Schneider T, Beck H and Matuttis H G 1996 *Phys. Rev.* B **54** 1286
[14] Kagan M Y, Fresard R, Capezzali M and Beck H 1998 *Phys. Rev.* B **57** 5995
[15] Metzner W and Vollhardt D 1989 *Phys. Rev. Lett.* **62** 324
[16] Walecka J D and Fetter A L 1971 *Quantum Theory of Many-Particle Systems* (New York: McGraw-Hill) p 131
[17] Thouless D J 1960 *Ann. Phys., NY* **10** 553
Also see
Ambregaokar V 1996 *Superconductivity* vol 1, ed R D Parks (New York: Dekker) p 259
[18] Serene J W 1989 *Phys. Rev.* B **40** 10 873
[19] Zubarev D N 1960 *Usp. Fiz. Nauk* 71 section 25
Zubarev D N 1960 *Usp. Fiz. Nauk* 71 section 31
[20] Walecka J D and Fetter A L 1971 *Quantum Theory of Many-Particle Systems* (New York: McGraw-Hill) p 297
[21] Lehmann H 1954 *Nuovo Cimento* **11** 342
[22] Tyablikov S V 1967 *Methods in the Quantum Theory of Magnets* (New York: Plenum)

[23] Georges A, Kotliar G, Krauth W and Rozenberg M J 1996 *Rev. Mod. Phys.* **68**
[24] Note that we are studying a system that would display s-wave pairing, and thus one does not require the k-resolved density of states to see evidence of a pseudo-gap.
[25] Serene J W and Vidberg H J 1977 *J. Low Temp. Phys.* **29** 179
[26] Demler E, Zhang S C, Bulut N and Scalapino D J 1996 *Int. J. Mod. Phys.* B **10** 2137
[27] Janko B, Maly J and Levin K 1997 *Phys. Rev.* B **56** R11 407
[28] Engelbrecht J R, Nazarenko A, Randeria M and Dagotto E 1997 *Phys. Rev.* B **57** 13 406
[29] Ulmke M 1998 private communication
[30] Letz M, Marsiglio F and Gooding R J 1998 in preparation